AUTOMATIC RECOGNITION OF MSTAR TARGETS USING RADAR SHADOW AND SUPERRESOLUTION FEATURES

Jingjing Cui, Jon Gudnason, Mike Brookes

Department of Electrical and Electronic Engineering
Imperial College London

ABSTRACT

Automatic target recognition from high range resolution radar profiles remains an important and challenging problem. In this paper, we present a novel feature set for this task that combines a representation of the target's radar shadow with a noise-robust superresolution characterisation of the target scattering centres derived from the MUSIC algorithm. Using an HMM to represent aspect dependence, we demonstrate that the inclusion of the shadow features results in a significant improvement in recognition performance. We evaluate our proposed feature set on a closed-set identification task using targets from the MSTAR database and show that it results in lower recognition error rates than previously published methods using the same data.

1. INTRODUCTION

The automatic detection and classification of targets from their radar signatures is an important and difficult problem that has attracted considerable research effort. Algorithms for target recognition from high range resolution (HRR) radar signals generally use as their primary input either a synthetic aperture radar (SAR) image or else a sequence of one or more one-dimensional range profiles. The image-based approaches generally have higher performance but are much less robust to target motion because of their long data acquisition time. Some image-based algorithms use the pixel values of the image as their recognition features [9, 10, 12] while others first transform the image to another domain [4, 16]. An alternative approach for targets that are large compared with the radar wavelength is to model the radar return as emanating from a discrete set of orientation-dependent points known as scattering centres [1]. In this approach, the SAR image is processed to generate an explicit list of scattering centre positions and associated radar cross sections on which the recognition features are based [2, 8]. In the same way, systems that act on the one-dimensional range profiles can either use the raw [18] or transformed [7] profile values as their features or else can process the profiles to estimate the scattering centre locations and cross sections [5]. Both SAR images and HRR profiles often exhibit large variations for small changes in target orientation. Target recognition systems must account for this aspect-dependency by using a rotation invariant transform [4] or by having multiple, orientation-dependent, target representations which may conveniently be embedded in an HMM [5, 13, 16].

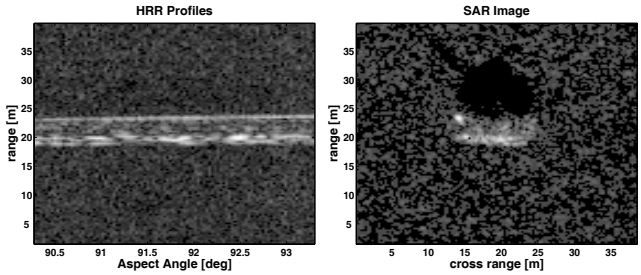

Fig. 1. (a) HRR profiles (b) SAR image of T72 tank

In this paper, we present a novel feature set for automatic target recognition from a sequence of radar range profiles. Our feature set uses a noise-robust super-resolution technique for identifying scattering centre locations and combines this information with additional features that characterise the shape of the radar shadow. Fig. 1 (b) shows a SAR image of a T72 tank taken from the MSTAR [14, 15] dataset. This image may be divided into three regions having significantly different characteristics: (a) the target itself characterised by discrete scattering centres within a relatively uniform background, (b) the target shadow with very low signal levels and (c) a clutter region surrounding the target. As can be seen in this example, the shape of the shadow region gives potentially useful information about the vertical profile of a target that is sited on level ground. This information is not available from the direct target returns which are insensitive to vertical displacement. The shadow information has been used by others to improve target detection [6] but is not generally used explicitly in target recognition.

This work was supported by the UK MoD through work funded by the Defence Technology Center for Data and Information Fusion.

In Section 2 of this paper, we describe our proposed feature set in detail and in Section 3, we describe the Hidden Markov model that we use to represent the aspect dependency of the radar returns. In Section 4 we evaluate the performance of our target recognition system using observation data from the MSTAR database [15] and compare its performance with that of other systems from the literature that use the same database. Finally, we summarise our results in Section 5.

2. RECOGNITION FEATURE SET

The features that we use for target recognition are derived from the sequence of complex-valued HRR profiles, $x(n,k)$, obtained by applying a discrete Fourier transform (DFT) to the windowed phase history radar returns. Here n is the profile index and k is the range-bin index covering the region of interest. Fig. 1(a) shows a typical plot of $|x(n,k)|$ and Fig. 1(b) shows the SAR image that results from windowing $x(n,k)$ and taking the DFT with respect to n. Visible in the image are the target itself, with signal levels well above the clutter noise level and also a well defined shadow region with very low signal levels. For each value of the profile index n, we obtain a feature vector, $\mathbf{u}(n)$, that characterises the positions and intensities of the scattering centres within the target and another, $\mathbf{w}(n)$, that characterises the shape of the shadow area. Both these feature vectors are derived from $2P+1$ consecutive profiles centred on profile n. We therefore define the data matrix $x_n(p,k) = x(n+p,k)$ where $p \in \{-P,\ldots,P\}$. The derivation of $\mathbf{u}(n)$ and $\mathbf{w}(n)$ is illustrated in Fig. 2 and the processing steps are described below where, for clarity, we omit the profile index, n. Each

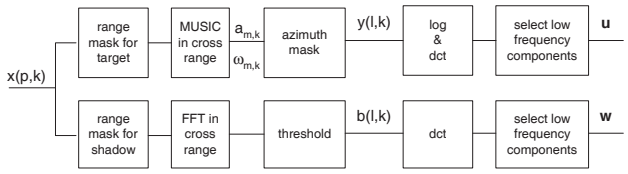

Fig. 2. Procedure to calculate features from HRR profiles

scattering centre in range bin k gives rise to a complex exponential term in $x(p,k)$ and the first step in obtaining $\mathbf{u}$ is to identify these terms. We do this by applying the MUSIC algorithm [17] which uses the data model

$$x(p,k) = \sum_{m=1}^{M} a_{m,k} exp(j\omega_{m,k}p) + v(p,k) \qquad (1)$$

where $a_{m,k}, \omega_{m,k}$ are the complex amplitudes and frequencies of the scattering centre terms and $v(p,k)$ is assumed to be white noise. The reasons for using the MUSIC algorithm are that it is resistant to noise, does not require windowing of $x(p,k)$ and is able to estimate $\omega_{m,k}$ with high

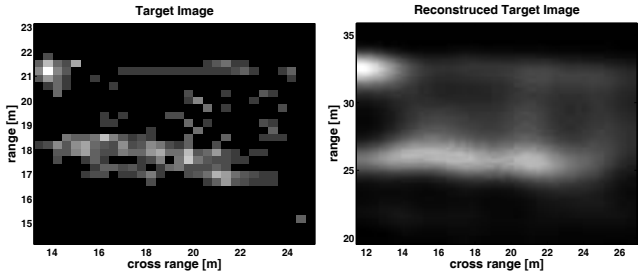

Fig. 3. (a) The image $y(l,k)$ (b) The image reconstructed using $\mathbf{u}$

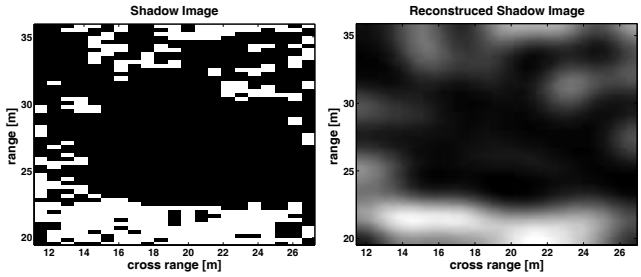

Fig. 4. (a) The two level shadow image, $b(l,k)$ (b) The image reconstructed using $\mathbf{w}$

resolution independently of P. Within range bin k, each of the M components in (1) corresponds to a scattering centre whose cross-range displacement is proportional to $\omega_{m,k}$. The maximum number of scattering centres, M, could be chosen adaptively for each range bin but we have, in the experiments below, fixed it at 10.

After discarding any scattering centres whose displacement lies outside the target mask, we convert the continuous displacements, $\omega_{m,k}$, to discrete values. We create a continuous signal containing an impulse for each scattering centre which we then low-pass filter and sample to give

$$y(l,k) = \sum_{m=1}^{M} |a_{m,k}|^2 \, h(l - c\omega_{m,k}) \qquad (2)$$

where $h(l) = (0.33\pi l)^{-1} sin(0.33\pi l)$ is the low-pass filter response and $c = 0.5\lambda\,(2\pi\Delta\phi\Delta r)^{-1}$ is a constant with $\lambda, \Delta\phi, \Delta r$ the wavelength, azimuth increment and cross range resolution, respectively. Fig. 3 (a) shows an example of $y(l,k)$ corresponding to the central portion of the image shown in Fig. 1 (b). The final step in forming the feature vector is to compress the image information by taking the 2-dimensional discrete cosine transform (DCT) of $\log y(l,k)$ and to retain only coefficients in the low frequency triangle of size 10-by-10 with (0,0) omitted to form the 54-element feature vector $\mathbf{u}$. Fig. 3(b) shows the reconstructed image using only the retained coefficients. To compute the shadow shape feature vector, $\mathbf{w}$, we first form a SAR image by windowing $x(p,k)$, zero-padding to obtain the correct

cross-range resolution and taking the DFT in the p direction. We then apply an adaptive threshold to the resultant image to obtain a binary-valued image, $b(l,k)$, representing the shadow. Fig. 4 (a) shows the shadow image obtained from the data of Fig. 1 (b) and it can be seen that the shadow is well identified although some clutter remains. As with the scattering centre features, we compress the shadow image by taking a 2-dimensional DCT and retaining 54 low frequency coefficients to form the shadow feature vector, $\mathbf{w}$. The reconstructed image using $\mathbf{w}$ is shown in Fig. 4 (b).

3. AZIMUTH HIDDEN MARKOV MODEL

HRR profiles exhibit significant variability with target orientation. We model this for each target using an HMM containing S states which correspond to different target aspects. Within an observation sequence, consecutive HRR profiles correspond either to the same or adjacent states. Thus the only allowable state transitions are from a state to itself or to the adjacent state in the direction of sensor motion.

We initialise the states to correspond to equal aspect increments of $360^\circ S^{-1}$ and for each state we train a Gaussian mixture model (GMM) [3] using all available training data from the corresponding range of aspects. The transition probability between adjacent states is initialised to be $S\Delta\phi/360^\circ$ where $\Delta\phi$ is the azimuth increment between successive feature vectors.

Using these initial values, we then re-estimate the GMM parameters and the HMM transition probabilities using embedded Baum-Welch training [19].

4. EXPERIMENTAL RESULTS

Our experimental evaluations make use of the Moving and Stationary Target Acquisition and Recognition (MSTAR) database collected by the Sandia National Laboratory using an X-band SAR sensor in 0.3m resolution spotlight mode [15, 14]. The database contains complex valued SAR image chips of 10 confusable targets and their variants. For each target, the images cover a full 360° azimuth range at depression angles of 15° and 17°. The SAR images have a resolution of $\Delta r = 0.3$m in both the range (vertical) and cross range (horizontal) directions.

For our experiments, the SAR image chips were converted into a sequence of HRR profiles [5]. Each chip covers an azimuth interval of approximately 3° [18] with successive HRR profiles separated by an angular increment of $\Delta\phi = 0.03^\circ$.

For our experiments we used an HMM containing $S = 60$ states each corresponding to an initial azimuth interval of 6°. Within each state, feature vector distributions are represented by a two-component diagonal-covariance Gaussian mixture model. We used a 9m $\times$ 9m target mask. For training, a total of 3000 image chips containing 17°-depression angle data was used to train the HMM. For testing, we used a total of 5000 15°-depression angle data without any compensation for the slight mismatch in depression angle.

Table 1. Recognition error rates (%)

	3° aperture			6° aperture		
Target	$\mathbf{u}$	$\mathbf{w}$	$\mathbf{u}+\mathbf{w}$	$\mathbf{u}$	$\mathbf{w}$	$\mathbf{u}+\mathbf{w}$
BMP2	6.7	34.0	2.6	3.5	34.3	0
BRDM2	1.1	16.1	6.2	1.1	4.8	0
BTR60	0	13.5	0	0	9.9	0
BTR70	3.6	34.0	8.2	4.1	25	4.4
D7	1.8	0.4	1.1	0	0	0
T62	4.4	1.5	1.1	0	0	0
T72	1.5	19.6	2.1	1.7	14.3	1.5
ZIL131	1.5	0	0	1.4	0	0
ZSU234	1.1	0.7	0.4	0	1.7	0
2S1	6.6	4.4	2.9	2.0	1.1	0.6
Average	3.8	12.4	2.5	1.4	9.1	0.6

We evaluated three alternative feature sets: the scattering centre features ($\mathbf{u}$), the shadow features ($\mathbf{w}$) and the concatenation of the two ($\mathbf{u}+\mathbf{w}$). The first two sets contain 54 elements while the last has 108. The feature vectors were formed using $P = 25$ corresponding to an aperture of 1.5°. For each identification experiment, we take a sequence of observations covering an azimuth aperture of either 3° or 6° and determine the model with the highest likelihood. Model training and recognition were performed using the HTK recognition software [19].

Table 1 shows the recognition error rate for a closed set identification tasks using 10 different targets for each of the three feature sets for both 3° and 6° azimuth apertures. The table lists the percentage error rate for each target as well as the average error rates. Using a 6° azimuth aperture we see that the $\mathbf{u}$ and $\mathbf{w}$ parameter sets give overall error rates of 1.4% and 9.1%. In both cases the errors are concentrated in a small number of poorly recognised targets and when the two feature sets are combined to form $\mathbf{u}+\mathbf{w}$ we find that the overall error rate is reduced to 0.6% with seven of the ten targets error-free.

When the azimuth aperture is reduced to 3°, the average error rate of all three feature sets increase. As before, the combined feature set ($\mathbf{u}+\mathbf{w}$) performs significantly better than either set individually and the overall error rate is only 2.5%. Note however that the inclusion of the $\mathbf{w}$ features increases the error rate for three of the targets.

The error rate of 2.5% obtained using a 3° aperture can be directly compared with other published results based on the MSTAR database with the same recognition task. In [11], the authors obtained error rates of 4.1% using an approach based on the SAR image and in [5] an error rate of 17.8% was obtained when performing recognition on the HRR profiles directly.

The MSTAR database contains 11 variants of the T72 tank and 3 variants of the BMP2 tank, manifested by different realisations of the fuel tank, antenna, etc [5]. To evalu-

Table 2. Error rates with unknown targets (%)

Target	Strict	Class	Class from [5]
BMP2-c21	7.6	0	6.1
BMP2-9563	29.1	3.2	7.0
BTR70	4.4	-	14.1
BRDM2	0	-	8.6
BTR60	0	-	13.7
D7	0	-	4.8
T62	0	-	9.0
T72-a04	3.7	0	2.9
T72-a10	0	0	3.4
T72-a62	11.6	0	3.9
T72-132	5 .5	1.5	7.6
ZIL131	0	-	10.3
ZSU234	0	-	8.5
2S1	0	-	4.7
BMP2-9566	-	9.0	37.5
T72-a05	-	2.0	14.5
T72-a07	-	2.3	16.1
T72-a32	-	3.4	22.9
T72-a63	-	0	15.9
T72-a64	-	6.5	31.7
T72-s7	-	28.4	17.1
T72-812	-	15.7	29.6

ate the robustness of our recogniser to these variations, we trained models on two BMP2 variants, four T72 variants and the eight other targets using the $\mathbf{u} + \mathbf{w}$ feature set. We then conducted recognition tests on all 22 targets in the database using a 6° azimuth aperture. If the recogniser identified an incorrect variant of the correct tank model, it was counted as an error in the "Strict" column of Table 2 but as a correct identification in the "Class" column.

For targets included in the training set, the average class error rate is 0.65% and in most cases the precise variant of a particular target was identified correctly. For the unseen variants listed in the lower section of the table, the average class error rate was 8.4% with over half of the errors arising from the T72-s7 and T72-812 tank variants.

The final column of Table 2 shows the "Class" error rates reported in [5] for the same task. We see that for all targets except T72-s7 the recognition performance for our proposed feature set is considerably better. We note however that since [5] bases its recognition on individual HRR profiles, it will be less sensitive to target motion than when feature set described here is used with a large value of P.

5. CONCLUSIONS

This paper has presented a novel radar target recognition technique combining two-dimensional target and shadow information. The new technique complements the SAR-ATR and HRR-ATR techniques by using a feature extraction method that is robust to noise and that can extract target and shadow information accurately with limited azimuth aperture length. The experimental results using MSTAR database indicate that the new technique can achieve superior performance than other published techniques.

6. REFERENCES

[1] R. Bhalla, H. Ling, J. Moore, D. J. Andersh, S. W. Lee, and J. Hughes, "3D scattering center representation of complex targets using the shooting and bouncing ray technique: a review," *IEEE Antennas and Propagation Magazine*, vol. 40, no. 5, pp. 30–39, 1998.

[2] H. Chiang, R. L. Moses, and L. C. Potter, "Model-based classification of radar images," *IEEE Trans. on Infromation Theory*, vol. 46, no. 5, pp. 1842–1854, 2000.

[3] A. P. Dempster, N. M. Laird, and D. B. Rubin, "Maximum Likelihood from Incomplete Data via the EM Algorithm," *Journal of the Royal Statistical Society*, vol. 39, no. 1, pp. 1–38, 1977.

[4] D. P. Kottke, F. Jong-Kae, and K. Brown, "Hidden Markov modeling for automatic target recognition," in *Proc. Thirty-First Asilomar Conference on Signals, Systems and Computers*, vol. 1, 1997, pp. 859–863.

[5] X. Liao, P. Runkle, and L. Carin, "Identification of ground targets from sequential high-range-resolution radar signatures," *IEEE Trans. on Aerospace and Electronic Systems*, vol. 38, no. 4, pp. 1230–1242, 2002.

[6] P. Lombardo, M. Sciotti, and L. M. Kaplan, "SAR prescreening using both target and shadow information," in *Proc. Radar Conference*, 2001, pp. 147–152.

[7] D. E. Nelson, J. A. Starzyk, and D. D. Ensley, "Iterated wavelet transformation and signal discrimination for HRR radar target recognition," *IEEE Trans. on Systems, Man and Cybernetics, Part A*, vol. 33, no. 1, pp. 52–57, 2003.

[8] C. Nilubol, Q. H. Pham, R. M. Mersereau, M. J. T. Smith, and M. A. Clements, "Hidden Markov modelling for SAR automatic target recognition," in *Proc. IEEE Int. Conf. Acoustics, Speech, Signal Processing*, vol. 2, 1998, pp. 1061–1064.

[9] L. M. Novak, "A comparison of 1D and 2D algorithms for radar target classification," in *IEEE International Conference on Systems Engineering*, 1991, pp. 6–12.

[10] L. M. Novak, S. D. Halversen, G. Owirka, and M. Hiett, "Effects of polarization and resolution on SAR ATR," *IEEE Trans. on Aerospace and Electronic Systems*, vol. 33, no. 1, pp. 102–116, 1997.

[11] L. M. Novak, G. J. Owirka, and A. L. Weaver, "Automatic target recognition using enhanced resolution SAR data," *IEEE Trans. on Aerospace and Electronic Systems*, vol. 35, no. 1, pp. 157–175, 1999.

[12] J. A. O'Sullivan, M. D. DeVore, V. Kedia, and M. I. Miller, "SAR ATR performance using a conditionally Gaussian model," *IEEE Trans. on Aerospace and Electronic Systems*, vol. 37, no. 1, pp. 91–108, 2001.

[13] B. Pei and Z. Bao, "Radar target recognition based on peak location of HRR profile and HMMs classifiers," in *Proc. Radar Conference*, 2002, pp. 414–418.

[14] T. D. Ross and J. C. Mossing, "The MSTAR Evaluation Methodology," *Proc. SPIE - The International Society for OpticalEngineering*, vol. 3721, pp. 705–713, 1999.

[15] T. Ross, S. Worrel, V. Velten, J. Mossing, and M. Bryant, "Standard SAR ATR evaluation experiments using the MSTAR public release data set," *Proc. SPIE - The International Society for OpticalEngineering*, vol. 3370, pp. 566–573, 1998.

[16] P. Runkle, L. H. Nguyen, J. H. McClellan, and L. Carin, "Multi-aspect target detection for SAR imagery using hidden Markov models," *IEEE Trans. on Geoscience and Remote Sensing*, vol. 39, no. 1, pp. 46–55, 2001.

[17] R. Schmidt, "Multiple emitter location and signal parameter estimation," *IEEE Trans. on Antennas and Propagation*, vol. 34, no. 3, pp. 276–280, 1986.

[18] R. Williams, J. Westerkamp, D. Gross, A. Palomion, and T. Fister, "Automatic target recognition of time critical moving targets using 1D high range resolution (HRR) radar," in *IEEE Radar Conference*, 1999, pp. 54–59.

[19] S. Young, G. Evermann, T. Hain, D. Kershaw, G. Moore, J. Odell, D. Ollason, D. Povey, V. Valtchev, and P. Woodland, *The HTK Book*. Cambridge University Engineering Dept, 2002. [Online]. Available: http://htk.eng.cam.ac.uk/prot-docs/HTKBook/htkbook.html